Proceedings of the Sustainable Research and Innovation Conference
JKUAT Main Campus, Kenya
6 - 7 October, 2021

STATCOM controller tuning to improve LVRT capability of grid connected wind power generating plants

Irene N. Muisyo, Prof. Stanley I. Kamau and Prof. Christopher M. Muriithi

***Abstract*—**The global drive towards utilization of renewable and sustainable energy systems is being accelerated by the increase in energy demand, environmental concerns, and the depletion of fossil fuel reserves. Of the main renewable energy resources, wind power has been recording tremendous growth over the last two decades. Among wind turbine concepts, the Doubly Fed Induction Generator (DFIG) is the most popular wind turbine system due to its efficiency, separately controllable active and reactive power, and relatively low power rating of its power electronic converter. However, the DFIG is sensitive to power system faults since its stator is directly connected to the grid. With the high penetration level of wind power generating plants in grids, disconnecting Wind Power Plants (WPPs) during grid faults can affect stability of power systems. Power system operators have therefore set new grid codes which require wind farms to have Low Voltage Ride Through (LVRT) capability, hence contribute to system stability during grid faults. This paper utilizes a Static Synchronous Compensator (STATCOM) to enhance the LVRT capability of a 9 MW DFIG based WPP during grid faults. The ability of the test system to ride through voltage sags on the grid side is investigated with incorporation of a conventional STATCOM and further with a Particle Swarm Optimization (PSO) tuned STATCOM. Simulations are carried out in MATLAB programming software, using SimScape toolbox. Results show that the STATCOM tuned using PSO results in an improved LVRT capability for the WPP due to the dynamic injection of reactive power.

***Keywords*—**LVRT, PSO, STATCOM, VSC.

I. Introduction

OVER the last three decades, the utilization of renewable energy resources has been on the rise. This is attributed to the depletion of fossil fuel reserves, increase in energy demand, and environmental concerns. Wind energy is among the fastest growing renewable energy resources. The installed capacity of wind power generation globally was 744 GW by the end of 2020, which represented about 26% of renewable energy generation. China and US remain the world's largest onshore wind markets, together accounting for more than 60% of the new capacity in 2020 [1], [2]. Wind Turbine (WT) technologies have been evolving, with large wind turbines being developed to increase the maximum power capture at minimum cost. However, with large-scale integration of wind power generating plants into grids, challenges such as reliability and stability of power systems are intensified [2], [3]. Most wind turbines today are based on the Double Fed Induction Generator (DFIG), due to its advantages such as variable speed capability and independent active and reactive power control. However, the DFIG is sensitive to grid faults since its stator is directly connected to the power system. During grid faults, the transient stator flux sets up a surge current in the rotor circuit which can destroy the Power Electronic Converter (PEC). Voltage dips at the Point of Common Coupling (PCC) also reduces the converter capability to transfer power to the grid, which leads to increased DC-link capacitor voltage [4], [5].

The PEC is usually protected by a crowbar, which short-circuits the rotor once triggered by a fault. The DFIG thus operates as an induction generator, consuming reactive power from the grid, for magnetization. Reactive power consumption further contributes to voltage degradation. If the fault persists, the wind power generating plant is eventually disconnected from the grid [5], [6]. Previously, wind farms were allowed to disconnect from grids during power system faults. With increasing levels of wind power injection into grids, disconnecting wind power generation during faults can negatively impact the stability of a power system. Therefore, power system operators worldwide have revised their Grid Code Requirements (GCRs) to incorporate Low Voltage Ride Through (LVRT) capability of wind farms. LVRT capability is the ability of power plants to remain connected to the grid for a specific period during grid voltage sag conditions [3], [6].

Various techniques have been proposed in literature to improve the LVRT capability of DFIG based WPPs. The main methods often employed for LVRT capability enhancement of grid connected WPPs include utilization of crowbar circuits, braking resistors, Fault Current Limiters (FCLs) and recently, Flexible AC Transmission System (FACTS) devices [7], [8]. FACTS devices are power electronic based devices primarily used for steady-state control of active and reactive power flow into grids. Due to their reliability and fast response, FACTS devices are gaining popularity in their utilization to enhance large scale integration of renewable energy into grids. The Dynamic Voltage Restorer (DVR) and Static Synchronous Compensator (STATCOM) are the most utilized FACTS devices to enhance performance of grid connected WPPs.

I. N. Muisyo, Department of Electrical & Electronic Engineering, JKUAT (mobile phone: +254721332377; e-mail: muisyoirene@jkuat.ac.ke).

S. I. Kamau, Department of Electrical & Electronic Engineering, JKUAT.
C. M. Muriithi, School of Engineering & Technology, Murang'a University of Technology.

In this study, a STATCOM is incorporated in a power system with a DFIG based WPP, and LVRT capability investigated. The conventional STATCOM operation is based on fixed gains. From literature, very little has been done on the tuning of FACTS controllers using metaheuristic optimization algorithms. The main contribution of this work is the optimization of gain parameters of the STATCOM controller, using Particle Swarm Optimization (PSO). The test system will be subjected to symmetrical and asymmetrical faults independently, and LVRT capability investigated for conventional, and PSO tuned STATCOM.

Section II of the paper presents DFIG modelling, LVRT GCR, and the STATCOM operation. Section III gives the test system, STATCOM integration and tuning. Section IV presents the simulation results whereas conclusions and recommendations are given in section V.

II. WIND ENERGY CONVERSION SYSTEMS (WECS)

Wind Energy Conversion Systems (WECS) convert the kinetic energy in wind into mechanical energy, by means of wind turbine rotor blades. The mechanical power developed by a wind turbine depends on the wind velocity and air density, expressed as

$$P_m = \frac{1}{2}\rho A_r {v_w}^3 C_p(\lambda, \beta) \qquad (1)$$

where ρ is the air density ($\mathrm{kg/m^3}$), $A_r(\pi R^2)$ is the area swept by rotor blades ($\mathrm{m^2}$), v_w is the wind speed (m/s), C_p is the power coefficient which is a function of Tip-Speed Ratio (TSR) λ, and the blade pitch angle (β) [4], [9]. The mechanical energy is then converted into electrical energy, which is fed to the grid.

WECS are either based on Fixed Speed Wind Turbines (FSWT) or Variable Speed Wind Turbines (VSWT). The FSWT configuration is simple but is unable to extract maximum power at varying wind speed, since its slip can only be varied over a very small range. Most wind turbines today are based on the Variable Speed Wind Turbine (VSWT) technology, which utilizes power electronics to achieve an improved efficiency and reduced mechanical stress for a wider range of wind speeds. The most common VSWT is the Double Fed Induction Generator (DFIG), due to its advantages such as variable speed capability, independent active and reactive power control, lower converter cost, and lower active power losses [10], [11].

A. DFIG operation and control

The DFIG has its stator directly connected to the grid, while its rotor is connected to the grid through a Power Electronic Converter (PEC), as shown in Figure 1 [3].

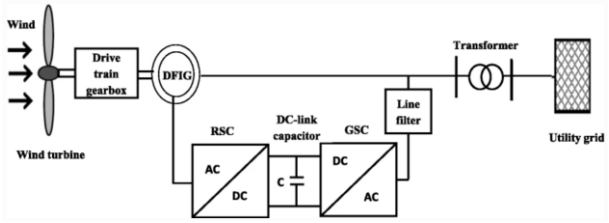

Figure 1: DFIG wind turbine.

In Figure 1, the Rotor Side Converter (RSC) controls active and reactive power flow from the stator to the grid while the Grid Side Converter (GSC) maintains the DC link voltage constant, thus controlling the grid current [3], [4]. The equivalent circuit of a DFIG in the d-q reference frame is shown in Figure 2.

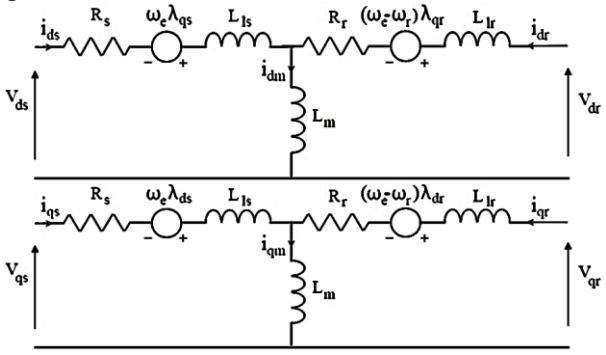

Figure 2: DFIG equivalent circuit.

From Figure 2, subscripts d and q indicate direct and quadrature axis components, whereas s and r indicate stator and rotor quantities, respectively [12]. The d and q stator and rotor flux components are:

$$\begin{aligned} \lambda_{ds} &= L_s i_{ds} + L_m i_{dr} \\ \lambda_{qs} &= L_s i_{qs} + L_m i_{qr} \\ \lambda_{dr} &= L_m i_{ds} + L_r i_{dr} \\ \lambda_{qr} &= L_m i_{qs} + L_r i_{qr} \end{aligned} \qquad (2)$$

where L_s and L_r are the stator and rotor inductances respectively, obtained using:

$$\begin{aligned} L_s &= L_{ls} + L_m \\ L_r &= L_{lr} + L_m \end{aligned} \qquad (3)$$

L_{ls} and L_{lr} are the stator leakage and rotor self-inductances respectively and L_m is the mutual inductance [12], [13]. The dq stator and rotor voltages are:

$$\begin{aligned} v_{ds} &= R_s i_{ds} + \frac{d\lambda_{ds}}{dt} - \omega_e \lambda_{qs} \\ v_{qs} &= R_s i_{qs} + \frac{d\lambda_{qs}}{dt} + \omega_e \lambda_{ds} \\ v_{dr} &= R_r i_{dr} + \frac{d\lambda_{dr}}{dt} - (\omega_e - \omega_r)\lambda_{qr} \\ v_{qr} &= R_r i_{qr} + \frac{d\lambda_{qr}}{dt} - (\omega_e - \omega_r)\lambda_{dr} \end{aligned} \qquad (4)$$

where, v and i denote voltage and current, respectively, R is the resistance (Ω), λ is the flux linkage (V·s), ω_e is the supply angular frequency (rad/sec), ω_r is the rotor angular frequency (rad/sec) [14], [15].

B. DFIG behavior during grid faults

Power system faults usually manifest as voltage sags, voltage swells, frequency fluctuations and blackouts. When a short-circuit fault occurs on the grid, a voltage sag or swell propagates to the Point of Common Coupling (PCC) of the WPP. The voltage variation results in a transient stator flux which causes a large electromotive force to be induced in the rotor circuit. The induced component is a multiple of the supply frequency. The severe the fault, the higher the magnitude of rotor current harmonics. A surge current in the rotor circuit can destroy the

Power Electronic Controller (PEC) devices. In addition, low voltage at the PCC reduces the capacity of the GSC to transfer active power to the grid. This leads to excess power in the DC-link capacitor, resulting in increased DC link voltage [15], [16]. Conventionally, the PEC is usually protected from rotor over currents using a crowbar. A crowbar consists of a set of switches usually activated upon fault occurrence, to bypass the RSC as shown in Figure 3 [13].

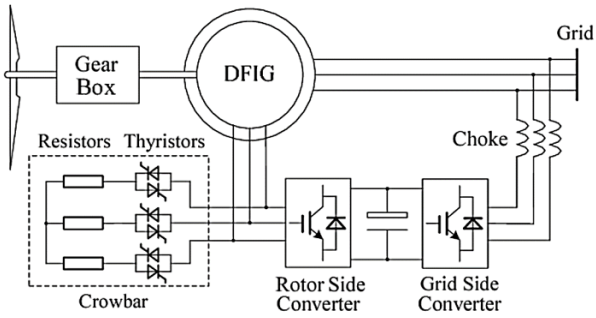

Figure 3: DFIG with crowbar resistance.

As shown in Figure 3, the crowbar circuit is usually implemented between the rotor circuit and the RSC to provide a bypass for the high transient rotor current, during faults. Once triggered by DC capacitor overvoltage or rotor overcurrent, the crowbar short-circuits the RSC, thus control of active and reactive power is lost. During this period, the DFIG absorbs reactive power from the grid, which negatively impacts voltage at the PCC. If the fault persists, the DFIG is finally disconnected from the grid [13], [15].

C. Fault ride through capability

Due to the significant increase in grid connected wind power generation, disconnecting large WPPs from a power system during disturbances can contribute to instability. Many countries have recently revised their grid codes to address the challenges of increased penetration of large wind power generation in modern power systems. Power system operators have identified Fault Ride Through (FRT) capability during disturbances as the most important Grid Code Requirement (GCR) in wind power integration into grids. FRT refers to the capability of power plants to remain connected to the grid during faults and provide reactive power support during such grid disturbances. FRT grid codes differ for each country based on the Transmission System Operator (TSO) requirements and grid strength. FRT capability has two aspects i.e., High Voltage Ride Through (HVRT) during voltage swells, and Low Voltage Ride Through (LVRT) during voltage sags. Voltage sags are the most common power system faults, hence LVRT is the most significant GCR when integrating wind power generation into grids [12], [17].

D. LVRT capability

Low Voltage Ride Through (LVRT) capability is demonstrated by profiles of voltage and time duration for which a generator must stay connected or disconnected from the grid, based on reduction in the voltage levels during faults. LVRT characteristics for various countries are shown in Figure 4 [12].

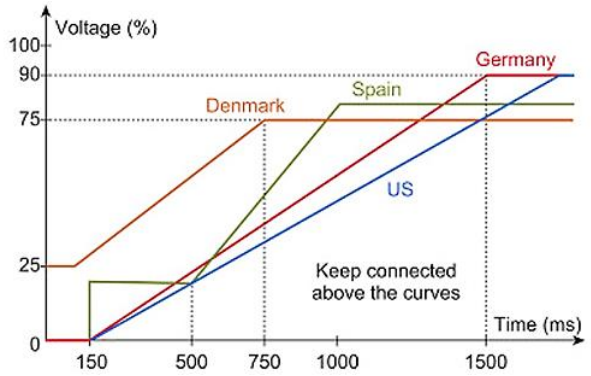

Figure 4: LVRT requirements for various countries.

From Figure 4 for instance, all wind farms connected to the German electric utility must withstand voltage drops up to 0% of nominal voltage at the PCC for a duration of 150ms. When the fault is cleared, voltage at the PCC should recover to 0.9p.u. within 1500ms [12], [18]. A summary of LVRT capability requirements for other countries is given in Table 1 [19].

Table 1: LVRT capability requirements.

S. No.	Country	Fault period		After fault clearance	
		T_{max}	V_{min}	T_{max}	V_{min}
1.	Denmark	100ms	25%	750ms	75%
2.	Ireland	625ms	15%	3000ms	90%
3.	Germany	150ms	0%	1500ms	90%
4.	Spain	150ms	0%	1000ms	85%
5.	USA (WECC)	150ms	0%	1750ms	90%
6.	USA (FERC)	625ms	15%	3000ms	90%
7.	Canada	150ms	0%	1000ms	85%
8.	Australia	100ms	0%	2000ms	70%

In literature, several methods are being explored for enhancement of the LVRT capability of DFIG based wind power generating plants. These methods include use of:

i. A crowbar which provides an additional path for the rotor current, thus the DFIG stays connected to grid [20], [21].
ii. A DC chopper connected in parallel with the PEC to dissipate excessive energy thus suppress the DC-link capacitor voltage [17], [22].
iii. Series Dynamic Breaking Resistors (SDBR), activated during fault conditions to limit the rotor current, thus avoid DC-link capacitor overvoltage [20], [22].
iv. Flexible AC Transmission System (FACTS) devices such as DVR [23], [24], SVC [3] and STATCOM [25], [26].

The DVR is a series connected custom power device which can be used to inject a dynamically controlled voltage at the PCC of a wind power plant. The DVR has been gaining popularity recently, due to its robustness. However, its rating should be the same as the rated output of the WTG. Moreover, DVRs are very expensive due to many ancillary components required during installation [12], [27]. The STATCOM is a shunt FACTS device primarily used to supply or absorb reactive power to support a specified bus voltage magnitude. It can control output voltage independently of the AC system voltage, with a very fast response. STATCOM modules are

easier to incorporate in existing power systems since they are shunt devices and do not require system modification such as in series devices.

E. STATCOM operation and control

The STATCOM comprises of a VSC, DC source and a coupling transformer, connected in shunt with the grid as shown in Figure 5.

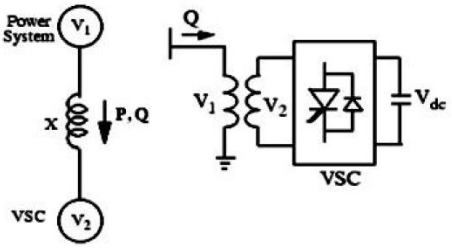

Figure 5: STATCOM schematic.

The VSC is the heart of a STATCOM consisting of self-commutating power electronic devices (GTO or IGBT), together with a reverse blocking diode in parallel. The DC capacitor provides DC input voltage, which is converted into a set of controllable three phase AC output voltages [8]. From Figure 5, V_1 is the bus voltage, V_2 is the VSC voltage, P is the active power of the VSC, Q is the reactive power of the VSC. If V_2 becomes less than V_1, Q flows from V_1 to V_2 and if V_2 becomes higher than V_1, Q will flow from V_2 to V_1. The VSC is driven by a controller which obtains DC link voltage V_{dc}, STATCOM reactive current I, and bus line voltage V_1, through a measurement system [28]. The STATCOM control system is shown in Figure 6.

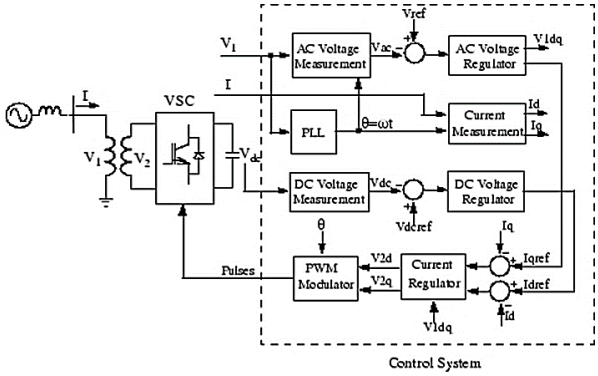

Figure 6: STATCOM control system.

As shown in Figure 6, the Phase Locked Loop (PLL) system generates synchronizing signals for *abc/dq0* transformation of the three-phase primary voltage (V_1) and current (I). The outer regulation loop consists of an AC voltage regulator and a DC voltage regulator. The output of the AC voltage regulator is the reference current I_{qref} for the current regulator. The output of the DC voltage regulator is the reference current I_{dref} for the current regulator. The inner current regulation loop consists of a current regulator which controls the magnitude and phase of the voltage generated by the PWM converter [28], [29]. The three regulators (AC voltage regulator, DC voltage regulator and the AC current regulator) are based on a Proportional Integral (PI) controller to regulate the STATCOM output. PI controllers provide a simple design structure at an affordable cost, which makes them popular in many industrial applications. The general form of a PI controller is:

$$U(t) = K_P e(t) + K_I \int e(t)dt \qquad (5)$$

where $U(t)$ represents the control signal, *e(t)* is the error signal, K_p and K_I are the proportional and integral gains respectively [30], [31]. The procedure of finding values of K_p and K_I which would result in the desired performance is called tuning. Controller tuning can be done using conventional methods such as Ziegler-Nichols (Z-N) and graphical tuning, or by intelligent optimization algorithms such as Fuzzy Logic (FL) based control, Genetic Algorithm (GA) and Particle Swarm Optimization (PSO) methods. For systems which are non-linear, time varying, or characterized by model uncertainties and/or disturbances, fixed gain PI controllers based on conventional tuning perform poorly [32].

With the advancement of artificial intelligence technologies, various optimization algorithms are increasingly being applied in controller parameter tuning and optimization. Intelligent optimization algorithms have merits of robustness and universality, but they also have some challenges such as premature convergence or slow convergence rate [30]. In this work, PSO will be used to tune the three PI STATCOM regulators, and the performance of the PSO-PI tuned STATCOM compared with that of a conventional STATCOM.

F. PSO-PI tuned STATCOM

Particle Swarm Optimization (PSO) is a biologically inspired computational search and optimization method developed in 1995 by Eberhart and Kennedy. The algorithm simulates the flight behavior of birds to find the place with the most adequate food. The PSO algorithm is illustrated in Figure 7 [19].

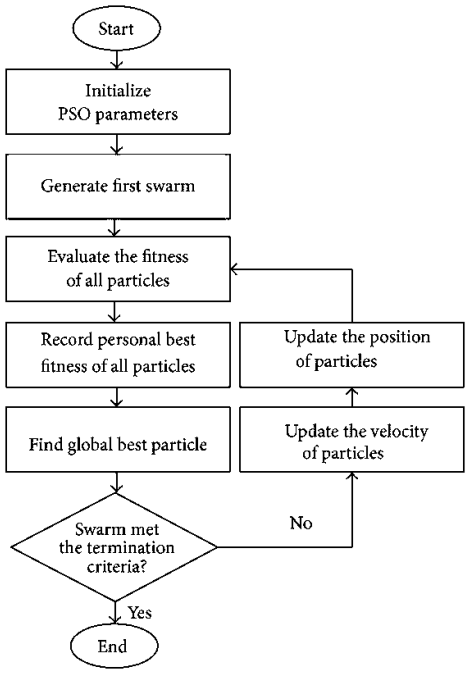

Figure 7: PSO flowchart.

As shown in Figure 7, the PSO algorithm starts by randomly generating particles (first swarm) in the search space. Next, the fitness value of each particle is evaluated, and the position corresponding to the best fitness value is called the local best position. The local best of all particles is compared and the best position in the swarm is defined as global best. At every iteration, the termination criteria are checked, and if not met, an update of the velocity and position of all particles is done [19], [33]. The velocity of particles is given by,

$$V_{k+1}^{i} = wV_k^i + C_1 r_1\left(P_k^i - X_k^i\right) + C_2 r_2\left(P_k^g - X_k^i\right) \qquad (6)$$

while the position of individual particles is updated by,

$$X_{k+1}^{i} = X_k^i + V_{k+1}^i \qquad (7)$$

where, X_k^i is the particle position, V_k^i is the particle velocity, P_k^i is the individual particle best position, P_k^g is swarm best position, w is the weight inertia used to ensure convergence, C_1 and C_2 are the cognitive and social parameters while r_1 and r_2 are random numbers between 0 and 1 [19], [34]. The PSO algorithm has been gaining popularity in real power system optimization problems such as in Distributed Generation (DG) location and Economic Dispatch (ED) problems. The PSO algorithm has advantages such as robustness, simple structure, fast convergence and short computational time. Additionally, it is efficient for solving problems without accurate mathematical models. However, with the PSO algorithm, it is difficult to define initial design parameters, and sub-optimal solutions can be obtained if a particle gets stuck in a local optima, especially with complex problems [35], [36].

In this work, the PSO algorithm was utilized to optimize the STATCOM controller gains. The shortcomings of PSO algorithm were minimized by using the conventional STATCOM gain values as the initial parameters. STATCOM controller tuning was converted to an optimization problem, with the aim of minimizing voltage fluctuations at the PCC. The fitness function was taken as the error between the reference values and the measured value, represented by the Integral Time Absolute Error (ITAE). By utilizing the ITAE function, error signals are amplified by the time signal and integrated, then controller gains which minimize the error evaluated. The optimization problem (fitness function) is stated as,

minimize

$$J = \int_0^T t(i)(|V_{ref} - V_{bus}|)dt \qquad (8)$$

subject to

$$K_r^{min} \le K_r \le K_r^{max}$$

where V_{ref} and V_{bus} are the reference and measured voltages, at the STATCOM connection bus respectively, t is the time range of the simulation and K_r represents the controller gains.

III. METHODOLOGY

LVRT capability investigation was done for a power system integrated with a 9 MW DFIG based wind power generating plant, first with a conventional STATCOM and afterwards with a PSO tuned STATCOM. Simulations were carried out in MATLAB/Simulink programming software, using SimScape toolbox.

A. Test system

The test system was developed by aggregating six, 1.5 MW DFIG wind turbines into a 9 MW wind power plant. A single line diagram of the system is shown in Figure 8. The output of the wind power generating plant is injected into a 25kV distribution system through a three phase 12MVA transformer.

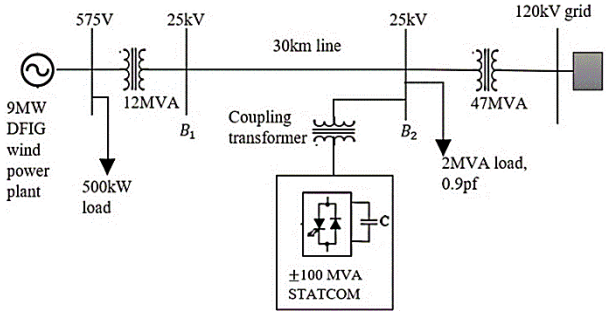

Figure 8: Single line diagram of test system.

A medium transmission line of 30km length connects the wind power generating plant to a 120kV grid through a three phase 47MVA transformer at bus feeder B_2. The DFIG WPP parameters and the system data is given in the Appendix as obtained from [26].

B. Conventional STATCOM integration

A STATCOM was installed at buses B_1 and B_2 independently, as voltage profile and reactive power injection was monitored, to determine the optimal location and size of the STATCOM. B_2 was obtained as the most optimal location, whereas the optimal size of the STATCOM was obtained as ± 100 MVA. A conventional 25kV, 100MVA STATCOM was adopted, whose classical gains and parameters obtained from [28] were used, presented in Table 2.

Table 2: Conventional STATCOM PI parameters.

S. No.	Specifications	Quantity
1.	Nominal voltage and frequency	500kV$_{L-L\,rms}$, 60Hz
2.	Converter rating	100MVA
3.	Converter impedance	R_1 = 0.00733 pu L_1 = 0.22 pu
4.	DC link nominal voltage	40kV
5.	DC link total equivalent capacitance	C=3000 µF
6.	Reference voltage	1 p.u.
7.	Droop	0.03 p.u.
8.	AC voltage regulator gains	$K_P = 5$ $K_I = 1000$
9.	DC voltage regulator gains	$K_P = 0.0001$ $K_I = 0.02$
10.	AC current regulator gains	$K_P = 0.3$ $K_I = 10$

C. PSO-PI tuned STATCOM

The PSO was used to tune gains of the three PI controllers in the STATCOM. The general objective function based on ITAE given in (8) was modified as

$$J(X) = \int_0^T |e_{Vac}|t\,dt + \int_0^T |e_{Iac}|t\,dt + \int_0^T |e_{Vdc}|t\,dt \qquad (9)$$

where $X = [K_{P1}, K_{I1}, K_{P2}, K_{I2}, K_{P3}, K_{I3}]$

K_{P1} and K_{I1} regulate the AC voltage controller, K_{P2}, K_{I2} regulate the current controller while K_{P3} and K_{I3} regulate the DC voltage controller. The PSO algorithm minimizes total ITAE error value and returns the final fitness value, and the corresponding six gains at the optimal output. The PSO parameters are given in Table 3.

Table 3: PSO parameters.

S. No.	Parameter name	Variable	Value
1.	Population size	n	100
2.	Maximum number of iterations	N	100
3.	Dimension (no. of parameters)	dim	6
4.	Minimum inertia weight	w_{min}	0.4
5.	Maximum inertia weight	w_{max}	0.9
6.	Cognitive component	C_1	1.4
7.	Social component	C_2	1.4
8.	Random numbers	r_1, r_2	U (0,1)

The algorithm begins with random initialization of K_P and K_I, then the fitness function is evaluated and checked against the desired value. The velocities and positions of the particles are updated based on (8) and (9), and the execution cycle continues until either the fitness function gets to the specified tolerance, or the maximum number of iterations are met. Gains of the conventional STATCOM controller given in Table 2 were used to initialize the algorithm, to ensure faster convergence and feasibility. The STATCOM gains obtained by PSO tuning are given in Table 4.

Table 4: PSO tuned STATCOM gains.

1.	AC voltage regulator gains	$K_P = 12$ $K_I = 3706$
2.	DC voltage regulator gains	$K_P = 0.001$ $K_I = 0.01$
3.	AC current regulator gains	$K_P = 5$ $K_I = 113$

IV. Results

The test system was independently subjected to L-G and LLL-G, 100% voltage sags on the grid side for 150ms. A constant wind speed of 12m/s is assumed, since the fault duration is very short, thus it does not allow noticeable speed variations. The simulation time was taken to be 20 seconds, and the faults were introduced at t = 15 seconds and cleared at t = 15.15 seconds. A crowbar and wind turbine protection scheme were also incorporated. Simulations were independently performed for before a STATCOM, with a conventional STATCOM and with a PSO tuned STATCOM.

A. Single line to ground (L-G) fault

1) Voltage profile at WPP terminals

The voltage profile at the WPP terminals is shown in Figure 9, for L-G 100% voltage sag of 150ms on the grid side.

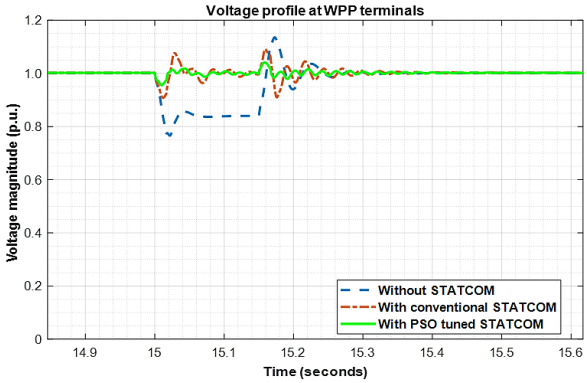

Figure 9: Voltage profile at WPP terminals.

At t=15s, a fault is simulated in which grid voltage drops to 0p.u. for 150s. During the fault period, the WPP terminal voltage drops from 1 p.u. to about 0.75p.u., before STATCOM incorporation. When the conventional STATCOM is incorporated, the voltage drops to about 0.9p.u., whereas for the case of a PSO tuned STATCOM, the voltage drops to about 0.95p.u. The conventional STATCOM injects about 80MVAr whereas the PSO tuned STATCOM injects about 90MVAr during the fault period at the point of connection.

Thus, with reference to the scenario before STATCOM incorporation, voltage fluctuations reduce by 20%, and 15%, with conventional, and PSO tuned cases, respectively. These findings agree with Hale Bakir and Ahmet Kulaksiz in [37], who use Genetic Algorithm (GA) and Bacteria Foraging Algorithm (BFA) to tune a STATCOM for the same test system.

From Figure 9, voltage at the WPP terminals has minimal voltage fluctuations during, and after fault clearance when a PSO tuned STATCOM is utilized. When the fault is cleared, the voltage rises momentarily to 1.15p.u., 1.1p.u., and 1.05p.u., without, with conventional, and with PSO tuned STATCOM installation, respectively. The overvoltage is caused by the excess reactive power supplied by the GSC and STATCOM during the fault period. The overvoltage can be reduced by incorporating fault current limiters to suppress the overshoots.

The voltage profile in Figure 9 can be compared with LVRT capability requirements for Germany and Canada, given in Table 1. LVRT capability requirements of the two countries state that grid connected wind power plants should be able to withstand voltage sags of up to 0% for 150ms. From Figure 9, this requirement has been met for the scenarios investigated.

2) WPP active power output

Figure 10 shows active power output of the WPP for L-G, 100% voltage sag of 150ms on the grid side.

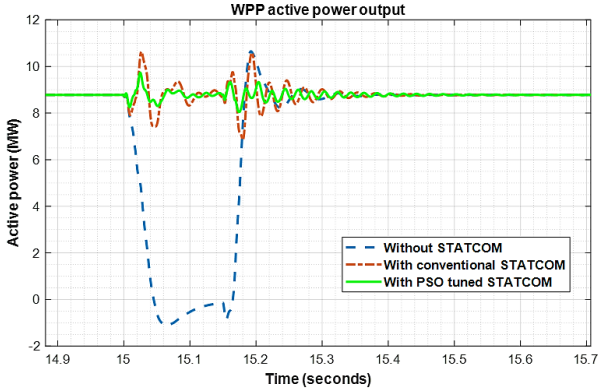

Figure 10: WPP active power output.

Without STATCOM incorporation, active power output at the WPP drops from 8.8MW to about -1MW, due to the low voltage on the connection bus. Once the DFIG protection system detects an undervoltage from 0.75p.u., the crowbar is activated (protection parameters are given in Table 8). The RSC is bypassed and the DFIG acts as a Squirel Cage Induction Generator (SCIG). As the voltage drops, active power supply to the grid falls to zero and the WPP draws active power from the grid. When either conventional or PSO tuned STATCOM is incorporated, voltage support is provided at the PCC, and the WPP maintains active power output during the fault period. As demonstrated in Figure 10, active power fluctuations are smallest when the PSO tuned STATCOM is utilized.

3) WPP reactive power output

Figure 11 shows the reactive power output of the WPP for L-G, 100% voltage sag of 150ms on the grid side.

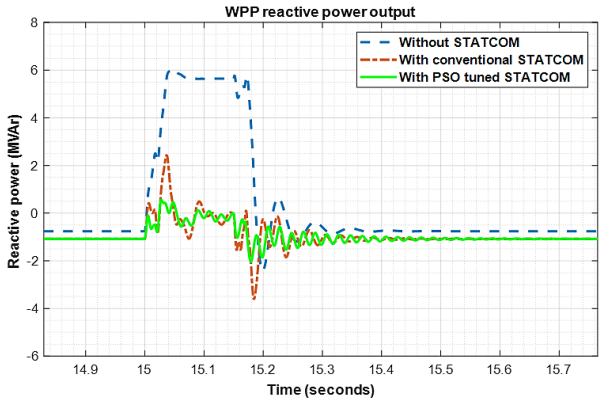

Figure 11: WPP reactive power output.

When the grid fault occurs, for the case without a STATCOM, the GSC injects up to 6MVAr to support the voltage at the WPP terminals. For the other two scenarios, both GSC and the STATCOM inject reactive power at the point of connection in an attempt to alleviate the undervoltage. The oscillations in reactive power during and after the fault are better damped when the PSO tuned STATCOM is incorporated as opposed to the conventional one. With help of the reactive power injection, action of the RSC is easily restored and the DFIG resumes normal operation rapidly.

4) DC link capacitor voltage

DC link capacitor voltage of the DFIG for L-G 100% voltage sag of 150ms on the grid side is shown in Figure 12.

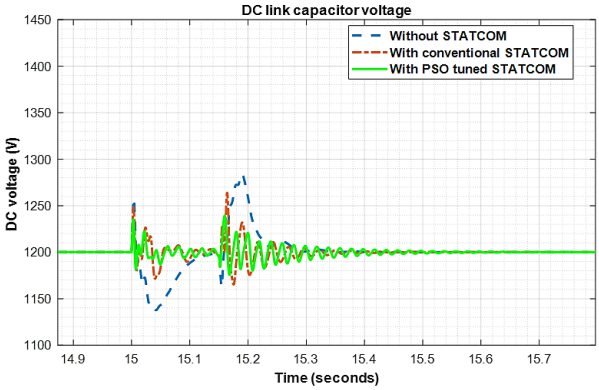

Figure 12: DC link capacitor voltage.

From Figure 12, the DC link capacitor voltage fluctuates from the reference value of 1200V to around 1250V at the onset of the voltage sag, and back to about 1280V at the end of the fault period, when a STATCOM is not utilized. When a conventional STATCOM is used, the fluctuations are reduced. The PSO tuned STATCOM results in the least fluctuations.

B. Three lines to ground (LLL-G) fault

1) Voltage profile at WPP terminals

The voltage profile at the WPP terminals is shown in Figure 13 for LLL-G 100% voltage sag of 150ms on the grid side.

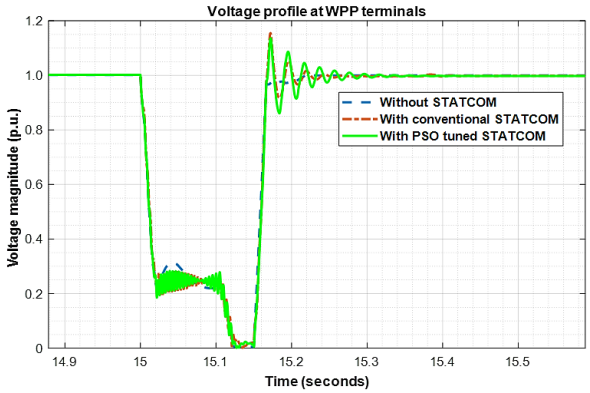

Figure 13: Voltage profile at WPP terminals.

At t=15s, voltage at the grid side falls to zero due to the LLL-G fault, and as seen in Figure 13, the WPP terminal voltage drops from 1 p.u. to 0p.u., for all three cases. Both conventional and PSO tuned STATCOM inject maximum reactive power of 110MVAr at the point of connection during the fault period, but the WPP still gets disconnected at t=15.12s. Disconnection of the WPPs is attributed to an undervoltage detected by the protection system. When the fault is cleared, the voltage rises momentarily up to about 1.15p.u. for both conventional and PSO tuned STATCOM utilization. The overvoltage is due to the reactive power supplied by the STATCOM during the fault period. The transients last for about 150ms after fault clearance, and a steady state is reached.

The voltage profile given in Figure 13 is compared with LVRT capability requirements for Germany and Canada which state that grid connected wind power plants should be able to withstand voltage sags of up to 0% for 150ms. From Figure 13, this requirement has not been met for the three scenarios.

2) WPP active power output

Figure 14 shows active power output of the WPP for LLL-G, 100% voltage sag of 150ms on the grid side.

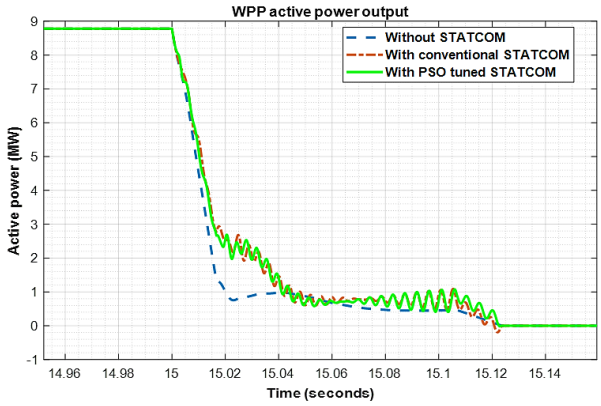

Figure 14: WPP active power output.

During the LLL-G fault, active power output at the WPP rapidly drops from about 8.8MW up to the point of disconnection at t=15.12s, due to the low voltage on the connection bus. For the three scenarios, the WPP gets disconnected and active power generation does not resume. Both conventional and PSO tuned STATCOM provide voltage support, but the fault is too severe thus the WPP still gets disconnected.

3) WPP reactive power output

Figure 15 shows reactive power output of the WPP for LLL-G, 100% voltage sags of 150ms on the grid side.

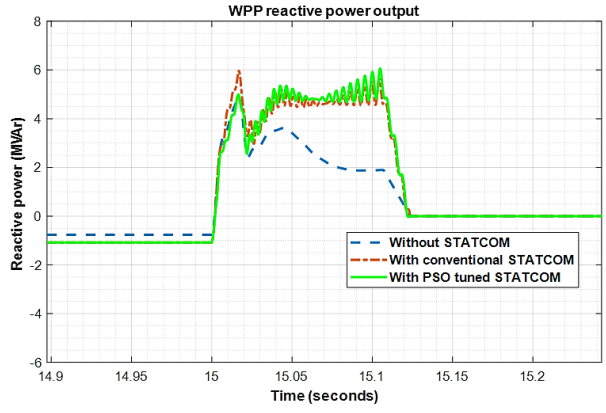

Figure 15: WPP reactive power output.

During the LLL-G grid fault, the GSC injects maximum reactive power into the grid of about 6MVAr, for the three scenarios, as shown in Figure 15. The DFIG thus acts to supply reactive power to the grid, in an attempt to aid grid recovery. Severe transients are observed at the beginning and end of the fault interval, which can be eliminated by using FCLs.

4) DC link capacitor voltage

Figure 16 shows DC link capacitor voltage of the DFIG for LLL-G, 100% voltage sag of 150ms on the grid side.

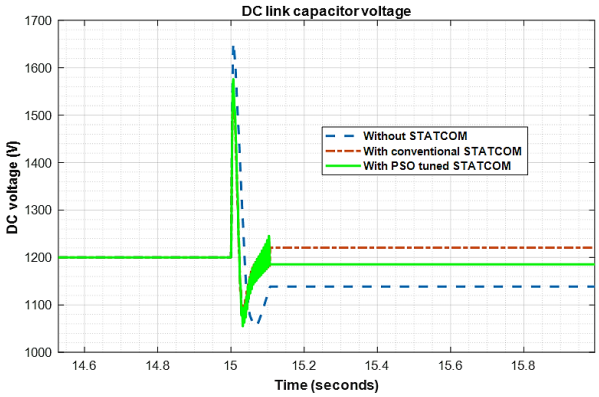

Figure 16: DC link capacitor voltage.

From Figure 16, the DC link voltage of the DFIG under the LLL-G fault drastically increases from its steady-state value of 1200V to a maximum of 1650V when a STATCOM is not connected. For the scenarios with STATCOM utilization, the DC link voltage remains high until the point of WPP disconnection from the grid.

V. Conclusion

In this work, LVRT capability of a grid connected 9MW DFIG based wind power generating plant was investigated against requirements of various countries. Simulations were carried out using MATLAB/Simscape toolbox. Performance comparison was done with both conventional and PSO tuned STATCOM in terms of the LVRT capability, active and reactive power, and DC link capacitor voltage, under L-G and LLL-G faults independently. It is observed that the PSO can be used to effectively tune the three controllers of a STATCOM, which results in enhanced LVRT capability of grid connected WPPs and improved dynamic performance.

During L-G faults, LVRT capability of Germany and Canadian power systems were met. However, the LLL-G faults were too severe for the WPP to ride through. Transients were observed at the beginning and end of fault period, whereby the PSO tuned STATCOM results in less voltage, active and reactive power overshoots. Voltage fluctuations reduce by 20%, and 15%, with conventional, and PSO tuned cases, respectively, during L-G faults, whereas during LLL-G faults, the voltage drops to zero during the fault period.

Since the STATCOM provides reactive power support, an additional technique of limiting the fault current can be incorporated, such as the FCL, SDBR or a DC chopper, to limit fault current, thus ensure the WPP meets LVRT capability requirements during LLL-G faults. STATCOM controller tuning using other metaheuristic optimization algorithms should be explored further and tested on practical systems.

APPENDIX

Table 5: Wind turbine parameters.

Wind turbine parameters	
Rated capacity	9MW (6 turbines x 1.5MW)
Cut-in wind speed	3.5ms/
Cut-out wind speed	25m/s
Rated wind speed	12m/s
No. of blades	3
Rotor diameter	82.5
Swept	5346m^2
Rotor speed	10.1-18.7 rpm

Table 6: Wind generator parameters.

DFIG parameters	
P_{rated}	9 MW
V_{rated}	575 V
r_s	0.00706
r_r	0.005
l_{ls}	0.171
l_{lr}	0.156
L_m	2.9
pf	0.9

Table 7: Transmission line parameters.

Transmission line parameters (π) model	
r_l	0.1153Ω/km
r_0	0.413Ω/km
l_l	0.00105H/km
l_0	0.00332H/km
C_l	$11.33e^{-9}$F/km
C_0	$5.01e^{-9}$F/km

Table 8: Wind turbine protection system.

Protection type	**Value**	**Delay**
AC overcurrent	$I_{1\,max} = 1.1$ pu	5sec
Maximum AC current unbalance	$\frac{I_2}{I_{1\,max}} = 0.4$ pu	0.25sec
AC undervoltage	$V_{1\,min} = 0.75$ pu	0.15sec
AC overvoltage	$V_{1\,max} = 1.1$ pu	0.15sec
AC voltage unbalance	$\frac{V_2}{V_{1\,max}} = 0.05$ pu	0.2sec
AC voltage unbalance	$\frac{V_0}{V_{1\,max}} = 0.05$ pu	0.2sec
Maximum DC voltage	$V_{max} = 1900$V	0.001sec

REFERENCES

[1] IRENA, "Renewable capacity statistics," International Renewable Energy Agency, Abu Dhabi, 2020.

[2] A. Ibrahim, S. Gawish, N. El-Amary and S. Sharaf, "STATCOM Controller Design and Experimental Investigation for Wind Generation System," *IEEE Access*, vol. 7, pp. 150453-150462, 2019.

[3] H. Rezaie and M. Hossein, "Enhancing voltage stability and LVRT capability of a wind-integrated power system using a fuzzy-based SVC," *Engineering Science and Technology, an International Journal*, vol. 22, pp. 827-839, 2019.

[4] D. Bhutto, J. Ansari and H. Bukhari, "Wind Energy Conversion Systems (WECS) Generators: A Review," in *International Conference on Computing, Mathematics and Engineering Technologies* , 2019.

[5] Y. Peng, Y. Li, Z. Xu, M. Wen, L. Luo, Y. Cao and Z. Leonowicz, "Power Quality Improvement and LVRT Capability Enhancement of Wind Farms by Means of an Inductive Filtering Method," *Energies*, vol. 9, no. 302, 2016.

[6] Y.-L. Hua, Y.-K. Wua, C.-K. Chen, C.-H. Wang, W.-T. Chen, Y.-L. Hua, Y.-K. Wua and C.-K. Chen, "A Review of the Low-Voltage Ride-Through Capability of Wind Power Generators," *Science Direct*, vol. 141, pp. 378-382, 2017.

[7] S. B. Naderi, P. Davari, D. Zhou, M. Negnevitsky and F. Blaabjerg, "A Review on Fault Current Limiting Devices to Enhance the Fault Ride-Through Capability of the Doubly-Fed Induction Generator Based Wind Turbine," *Journal of Applied Sciences*, vol. 8, no. 11, pp. 1-24, 2018.

[8] A. Karami and ·. M. Galougahi, "Improvement in power system transient stability by using STATCOM and neural networks," in *Springer Nature*, Germany, 2019.

[9] O. Noureldeen and I. Hamdan, "A novel controllable crowbar based on fault type protection technique for DFIG wind energy conversion system using adaptive neuro-fuzzy inference system," *Protection and Control of Modern Power Systems*, vol. 3, no. 35, pp. 1-12, 2018.

[10] D. Chauhan and S. Goel, "Designing of Advanced Crowbar Protection System for DFIG Coupled Wind Energy Conversion System at Different Fault Conditions," *International Journal of Science Technology & Engineering*, vol. 4, no. 11, pp. 119-125, 2018.

[11] S. Soued, H. Ramadan and M. Becherif, "Effect of Doubly Fed Induction Generator on Transient Stability Analysis under Fault Conditions," *Energy Procedia*, no. 162, p. 315–324, 2019.

[12] A. Benali, M. Khiat, T. Allaoui and M. Denai, "Power Quality Improvement and Low Voltage Ride Through Capability in Hybrid Wind-PV Farms Grid-Connected Using Dynamic Voltage Restorer," *IEEE Access*, vol. 6, no. 1, pp. 68634-68649, 2018.

[13] S. Zain and I. A. Ahmed Helal, "Low Voltage Ride through Capability Techniques for DFIG-based Wind Turbines," *International Journal of Energy and Power Engineering*, vol. 10, no. 7, pp. 910-919, 2016.

[14] R. Ann, P. Kaliannan, S. Padmanaban and V. Ramachandaramurthy, "Improved Fault Ride Through Capability in DFIG Based Wind Turbines Using Dynamic Voltage Restorer With Combined Feed-Forward and Feed-Back Control," *IEEE Access*, vol. 5, pp. 20494-204105, 2017.

[15] J. Mwaniki, H. Lin and Z. Dai, "A Concise Presentation of Doubly Fed Induction Generator Wind Energy Conversion Systems Challenges and Solutions," *Hindawi Journal of Engineering*, pp. 1-13, 2017.

[16] A. Parameswari and H. Sait, "A comprehensive review of fault ride-through capability of wind turbines with grid-connected doubly fed induction generator," *International Transactions on Electrical Energy Systems*, vol. etep12395, 2020.

[17] D. S and K. T, "Review of control strategies for DFIG wind turbine to enhance LVRT Capability," *International Journal of Innovative Science, Engineering & Technology*, vol. 2, no. 4, pp. 339-343, 2015.

[18] T. Atuwo, "Application of Optimized SFCL and STATCOM for the Transient Stability and LVRT Capability Enhancement of Wind Farms," *International Journal of Research and Engineering*, vol. 5, no. 6, pp. 422-429, 2018.

[19] O. Kamel, A. Diab, T. D. and M. Mossa, "A Novel Hybrid Ant Colony-Particle Swarm Optimization Techniques Based Tuning STATCOM for Grid Code Compliance," *IEEE Access*, vol. 8, pp. 41566-41587, 2020.

[20] R. A. Jerin, P. Kaliannan, U. Subramaniam and M. El-Moursi, "A Review on Fault Ride Through Solutions for Improving Transient Stability in DFIG based Wind Turbines," *IET Renewable Power Generation*, pp. 1-25, 2018.

[21] Y. QU, L. GAO, G. MA, H. SONG and S. WANG, "Crowbar resistance value-switching scheme conjoint analysis based on statistical

sampling for LVRT of DFIG," *Journal of Modern Power System Clean Energy*, vol. 7, no. 3, p. 558–567, 2019.

[22] B. Qin, H. Li, X. Zhou, J. Li and W. Liu, "Low-Voltage Ride-Through Techniques in DFIG-BasedWind Turbines: A Review," *Applied Sciences*, vol. 10, no. 2154, pp. 1-25, 2020.

[23] D. Zhang, H. Xu, L. Qiao and L. Chen, "LVRT capability enhancement of DFIG based wind turbine with coordination control of Dynamic Voltage Restorer and inductive Fault Current Limiter," *PLoS ONE*, vol. 14, no. 8, 2019.

[24] P. D. Chung, "Voltage Enhancement on DFIG Based Wind Farm Terminal During Grid Faults," *Engineering, Technology & Applied Science Research*, vol. 9, no. 5, pp. 4783-4788, 2019.

[25] A. Rashad, S. Kamel, F. Jurado, M. Nasser and K. Mahmoud, "ANN-Based STATCOM Tuning for Performance Enhancement of Combined Wind Farms," *Electric Power Components and Systems*, pp. 1-17, 2019.

[26] O. Makram, A. Diab, T. Duc and M. Mossa, "A Novel Hybrid Ant Colony-Particle Swarm Optimization Techniques Based Tuning STATCOM for Grid Code Compliance," *IEEE Access*, vol. 8, pp. 41566-41587, 2020.

[27] R. A. Jerin, P. K, U. S and T. D, "Power Quality Improvement of Grid Connected Wind Farms through Voltage Restoration Using Dynamic Voltage Restorer," *International Journal of Renewable Energy Research*, vol. 6, no. 1, 2016.

[28] Mathworks, "MATLAB programming software," 2018.

[29] G. Ahmed, Y. Mohmed and O. Kamel, "Optimal STATCOM Controller For Enhancing Wind Farm Power System Performance Under Fault Conditions," in *IEEE*, Cairo, 2016.

[30] Y.-Y. Hong, M.-T. Nguyen and H. Zeng, "Studies on Optimal Controller Design of STATCOM in Power System with Large Wind Farms," in *International Conference on Electrical Engineering*, Korea, 2018.

[31] S. Kumar, A. Rahman and R. Ahmed, "Tuning of PI and PID Controller with STATCOM, SSSC and UPFC for Minimizing Damping of Oscillation," *IOSR Journal of Electrical and Electronics Engineering*, vol. 12, no. 1, pp. 30-44, 2017.

[32] H. Wu, W. Su and Z. Liu, "PID controllers: design and tuning methods," in *IEEE Conference on Industrial Electronics and Applications*, Hangzhou, 2014.

[33] T.-Y. Wu, Y.-Z. Jiang, Y.-Z. Su and W.-C. Yeh, "Using Simplified Swarm Optimization on Multiloop Fuzzy PID Controller Tuning Design for Flow and Temperature Control System," *Applied Sciences*, vol. 10, pp. 1-23, 2020.

[34] T. Eswaran and S. Kumar, "Particle swarm optimization (PSO)-based tuning technique for PI controller for management of a distributed static synchronous compensator (DSTATCOM) for improved dynamic response and power quality," *Journal of Applied Research and Technology* , vol. 15, p. 173–189, 2017.

[35] A. Hossain, H. Roy, S. Squartini and A. Fathi, "Modified PSO algorithm for real-time energy management in grid-connected microgrids," *Renewable Energy*, vol. 136, pp. 746-757, 2019.

[36] Y. Zhang, L. Zhang and Z. Dong, "An MEA-Tuning Method for Design of the PID Controller," *Mathematical Problems in Engineering: Hindawi*, pp. 1-11, 2019.

[37] H. Bakir and A. Kulaksiz, "Modelling and voltage control of the solar-wind hybrid micro-grid with optimized STATCOM using GA and BFA," *Engineering Science and Technology, an International Journal* , vol. 23, p. 576–584, 2020.